African Geographical Review

ISSN: (Print) (Online) Journal homepage: https://www.tandfonline.com/loi/rafg20

Impacts of eco-environmental quality, spatial configuration, and landscape connectivity of urban vegetation patterns on seasonal land surface temperature in Harare metropolitan city, Zimbabwe

Pedzisai Kowe, Onisimo Mutanga, John Odindi & Timothy Dube

To cite this article: Pedzisai Kowe, Onisimo Mutanga, John Odindi & Timothy Dube (2022): Impacts of eco-environmental quality, spatial configuration, and landscape connectivity of urban vegetation patterns on seasonal land surface temperature in Harare metropolitan city, Zimbabwe, African Geographical Review, DOI: 10.1080/19376812.2022.2117215

To link to this article: https://doi.org/10.1080/19376812.2022.2117215

Published online: 02 Sep 2022.

AFRICAN GEOGRAPHICAL REVIEW
https://doi.org/10.1080/19376812.2022.2117215

Routledge
Taylor & Francis Group

Impacts of eco-environmental quality, spatial configuration, and landscape connectivity of urban vegetation patterns on seasonal land surface temperature in Harare metropolitan city, Zimbabwe

Pedzisai Kowe[a,b], Onisimo Mutanga[b], John Odindi[b] and Timothy Dube[c]

[a]Department of Geography, Environmental Sustainability and Resilience Building, Faculty of Social Sciences, Midlands State University, Gweru, Zimbabwe; [b]Discipline of Geography, School of Agricultural, Earth and Environmental Sciences, University of KwaZulu-Natal, Pietermaritzburg, South Africa; [c]Department of Earth Sciences, University of the Western Cape, Bellville, South Africa

ABSTRACT

The study examined the impact of eco-environmental quality conditions, spatial configurations and landscape connectivity of urban vegetation on seasonal land surface temperature (LST) in Harare, Zimbabwe between May and October 2018. The results showed that densely built-up areas with sparse vegetation experienced extremely poor eco-environmental conditions. Clustered and highly connected were more beneficial in decreasing LST. These findings have important urban and landscape planning implications regarding how the spatial configuration and landscape connectivity patterns of urban vegetation can be optimized to mitigate Urban Heat Island (UHI) effects and to improve the thermal comfort conditions in rapidly urbanizing cities.

ARTICLE HISTORY
Received 2 February 2022
Revised 1 August 2022
Accepted 18 August 2022

KEYWORDS
Spatial clustering; landscape pattern; local Moran's I; patch cohesion index; urban green space; seasons; urban heat island

1. Introduction

The global rapid expansion of urban areas has led to increases in land surface temperatures (LST) due to conversion of natural areas to built-up areas and impervious surfaces (Mallick et al., 2008). As the landscape becomes urbanized, the natural landscape gets fragmented, affecting its diversity and abundance as well as connectivity (Nor et al., 2017). Built areas and impervious surfaces have high thermal conductivity that significantly increases the heat storage capacity in cities, causing energy budget changes due to increased sensible heat (Oke, 1982; Voogt & Oke, 2003). Such changes lead to significantly warmer and higher temperatures in urban areas than the surrounding non-urban areas, creating an urban heat island phenomenon (UHI; Oke, 1982; Voogt & Oke, 2003).

UHI affect the daily lives of urban dwellers. UHI decreases air quality by increasing the production of pollutants such as ozone, whose formation further increases surface temperatures that may exacerbate the impact of heat waves in cities (Akbari et al., 2001; Fischer et al., 2007). Adverse effects of UHI are also known to increase electricity or energy consumption especially in hot and summer seasons (Yao et al., 2021). Furthermore, excess heat associated with UHI causes thermal discomfort in cities and among city dwellers, as well as increased health risks (Guha, 2021), resulting in heat-related diseases and premature deaths (Anderson & Bell, 2010; Jenerette et al., 2007). A city's thermal well-being and ecological or eco-environmental quality can be assessed by quantifying UHI and Urban Thermal Field Variance Index (UTFVI) data derived from remotely sensed LST (Guha, 2021).

CONTACT Pedzisai Kowe Kowemuso5@gmail.com

Consequently, urban green spaces are increasingly being used in urban planning and management to mitigate the adverse effects of UHI and to improve thermal comfort (Chen et al., 2012; Weng et al., 2004). In this regard, previous studies have extensively established a negative correlation between LST and vegetation cover using remotely sensed derivatives (Carlson et al., 1994; Voogt & Oke, 2003; Guha and Govil 2021a). Vegetation cover varies across seasons, subsequently affecting the energy balance and the thermal variability within an urban landscape (Zhang et al., 2015, 2003).

Mitigating UHI is therefore imperative. For example, optimizing the spatial configuration as defined in Zhou et al. (2011), of green spaces by holding spatial composition constant is crucial (Zhou et al., 2011). Similarly, green spaces and vegetation patches with more complex shapes and patch area based on landscape metrics like Mean Shape Index (MSI), Landscape Shape Index (LSI), Area Weighted Mean Shape Index (AWMSI), Area Weighted Mean Patch Fractal Dimension (AWMPFD), and Largest Patch Index (LPI) have been shown to deliver higher cooling effects (Bao et al., 2016; Cao et al., 2010; Connors et al., 2013; W. F. Li et al., 2017; Kong et al., 2014; Li et al., 2016; J. Li et al., 2011; Li et al., 2012; J. Peng et al., 2016; Zhang, Zhong, Feng et al., 2009; Zhibin et al., 2015; Zhou et al., 2011). Relating the landscape metrics to urban thermal responses of green spaces in a city is useful in capturing the effects of spatial configuration on the distribution and magnitude of LST through its effects on energy flows (Chen et al., 2016; Connors et al., 2013; W. F. Li et al., 2017; Kong et al., 2014; J. Peng et al., 2016).

However, many landscape metrics are highly correlated with each other, hence they are difficult to interpret (Li & Wu, 2004;Uuemaa et al., 2013) and may not be related to thermal processes in a city (Chen et al., 2016). Furthermore, it has been demonstrated that landscape metrics cannot fully represent the clustered and dispersed patterns of each land cover category (Fan & Myint, 2014). Many researchers have begun to explore the possibility of spatially explicitly characterizing land cover heterogeneity in urban landscapes derived from remotely sensed data using a continuous Local Indicators of Spatial Association (LISA) approach (Fan & Myint, 2014). Zheng et al. 2014 used the Local Moran's I index to characterize the influence of the spatial pattern of anthropogenic land cover on LST. The results of the study showed that clustered patterns of paved surfaces elevate LST and produce stronger warming effects at nighttime than daytime.

While the effects of spatial composition of urban vegetation on LST are well established (Chen et al., 2016, 2016; Connors et al., 2013; W. F. Li et al., 2017; Kong et al., 2014; J. Peng et al., 2016), there is a paucity in literature of how the spatial configuration of vegetation patterns affects the seasonal surface temperatures in rapidly growing African cities. Therefore, in this study, we aim to (1) determine the impact of spatial configuration and landscape connectivity patterns of green vegetation cover on seasonal daytime LST using the local Moran's I and Patch Cohesion Index derived from Landsat data and (2) evaluate the thermal ecological-environmental quality conditions of Harare metropolitan city using urban thermal field variation index (UTFVI).

2. Materials and methods

2.1 Study area

The study was conducted in Harare metropolitan city, Zimbabwe. Harare metropolitan city is situated on latitude 17.83°South and longitude 31.05° East (Figure 1). It is the political capital and the major center of industrial production, trade, and commerce. The city has an area of approximately 980.6 km^2 and 2.42 million people as per the 2022 population census (Zimstat, 2022). The city has witnessed rapid urbanization over the past few decades (Kamusoko et al., 2013), and the trend is expected to continue (Mushore et al., 2017). Such a rapid urbanization will inevitably generate adverse UHI effects, negatively impacting the provision of ecosystem services and the environmental quality.

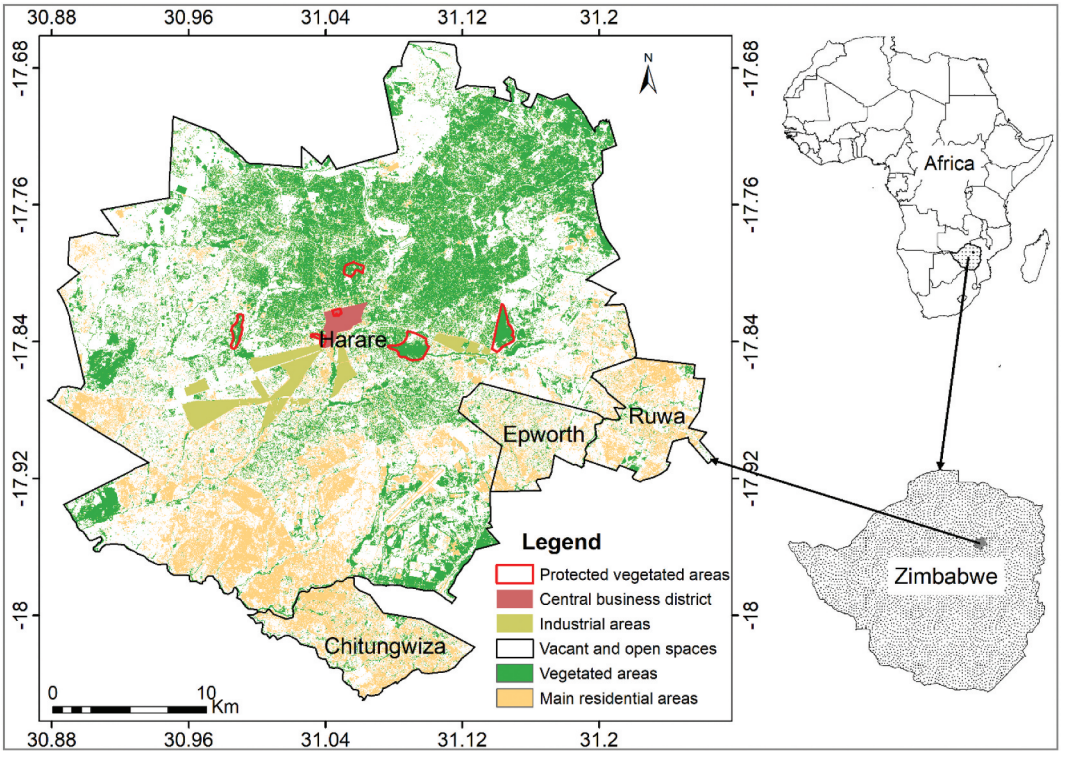

Figure 1. The geographical location of the study area.

Harare metropolitan city is mainly characterized by a flat and hilly topography in the southern and northern parts, respectively. The city falls within the subtropical highland climate, which is typically mild and cool with relatively longer sunshine hours. It experiences warm and hot summers and cold winters. Generally, there are four distinct seasons in the city (1) spring or transitional season from April to May (2), a cool and dry winter season from June to July (3), a relatively warm and dry season from August to September, and (4) a dry and wet summer season from October to March.

2.2 Satellite data acquisition

The Landsat 8 Operational Land Imager (OLI) and Thermal Infrared Sensor (TIRS) sensor data acquired in 2018 were used. Landsat 8 OLI optical bands of visible, near-infrared, short-wavelength infrared and cirrus bands have a spatial resolution of 30 m. The TIRS bands have two channels with (a spatial resolution of 100 m. The Landsat data series are the most widely used data source for retrieving LST (°C) for urban studies (Weng et al., 2004). These data have moderately high spatial resolution relative to other widely available thermal bands of sensors like 1 km Advanced Very High-Resolution Radiometer (AVHRR) and Moderate Resolution Imaging Spectroradiometer (MODIS).

Satellite images selected for this study were from May (spring, mild and cool), June (winter, cold and dry), August–September (cool and dry), October (hot and dry) to November (hot and wet). The selected satellite dates correspond to spring, winter, autumn, and summer seasons, respectively (Table 1). Due to the high amount of cloud cover over Harare, satellite images between December and April were excluded. The non-availability of suitable images of January, February, March, April, and December 2018 as a result of either cloud cover was not considered a major problem for

Table 1. Details of Landsat 8 (OLI/TIRS) satellite data acquisition.

Satellite sensor	Acquisition date	Season	Season conditions
Landsat 8	19 May 2018	Spring	Mild and cool
Landsat 8	20 June 2018	Winter	Cold and Dry
Landsat 8	23 August 2018	Autumn	Cool and dry
Landsat 8	24 September 2018	Autumn	Cool and dry
Landsat 8	26 October 2018	Summer	Hot and dry
Landsat 8	11 November 2018	Summer	Hot and wet (Rainy)

the study as representative seasons were available. The freely available satellite cloud-free images were downloaded from the United States Geological Survey (USGS) website (http://earthexplorer.usgs.gov/). Detailed information on the data (year or acquired date, satellite sensor, spatial resolution, season, and seasonal conditions) is shown in Table 1.

2.3. Computing and retrieving land surface temperature

LST was retrieved from image data captured between May 2018 and November 2018. Only Landsat 8 band 10 was used for the computation of LST as USGS discouraged the use of band 11 due to stray light from far out-of-field that interferes and affects the thermal data. The normal approach of retrieving LST from raw Landsat thermal imagery involves the conversion of the thermal band's Digital Number (DN) values into radiance associated with Landsat 8 band 10 according to radiometric rescaling coefficients (i.e., calibration coefficients) (Chander & Markham, 2003) using Equation (1).

$$L_{(\lambda)} = \frac{\left(LMAX_{(\lambda)} - LMIN_{(\lambda)}\right)}{\left(Q_{calmax} - Q_{calmin}\right)} \mathrm{x}(Q_{cal} - Q_{calmin}) + LMIN_{(\lambda)} \tag{1}$$

Where $L_{(\lambda)}$isthe spectral radiance at the sensor's aperture in W/(m^{2}sr μm)

Q_{cal} is the quantized calibrated pixel value [DN]

Q_calmix is the minimum quantized calibrated pixel value corresponding to $LMIN_{(\lambda)}$ [DN]

Q_calmax is the maximum quantized calibrated pixel value corresponding to $LMAX_{(\lambda)}$ [DN]

$LMIN_{(\lambda)}$ the spectral at-sensor radiance scaled to Q_calmix in W/(m^{2}sr μm) and

$LMAX_{(\lambda)}$ the spectral at-sensor radiance scaled to Q_calmax in W/(m^{2}sr μm)

The obtained radiance values were later converted to at-sensor or satellite brightness temperatures (Chander et al., 2009). The conversion formula from the at-sensor's spectral radiance to at-sensor brightness temperature is achieved by applying the inverse of the Planck radiance function for temperature. The Planck's Law is expressed as Equation (2)

$$T_B = \frac{K_2}{\ln\left(\left(\frac{K_1}{L_\lambda}\right) + 1\right)} \tag{2}$$

where T_B is the at-sensor brightness temperature in degrees Kelvin. L_λ is spectral radiance in $\mathrm{Wm^{-2}sr^{-1}mm^{-1}}$. The at-sensor temperature uses the pre-launch calibration constants K_1 and K_2. K_1 and K_2 are calibration constant 1 and 2 respectively. K_1 and K_2 values are 774.89 and 1321.08, respectively, for Landsat 8 thermal band 10. In the retrieval of LST values, the at-satellite brightness temperatures need to be scaled using land surface emissivity (ε) following the method developed by Sobrino et al. (2008) as expressed in Equation (3);

$$(\varepsilon) = \varepsilon_v P_{v+} \varepsilon_s (1 - P_v) + d\varepsilon \tag{3}$$

Where

ε_s = soil emissivity

ε_v = vegetation emissivity

Pv = Proportion of vegetation or fractional vegetation cover.

d_ε = the geometric distribution effects and internal reflections of natural surfaces (Guha et al., 2018).

In heterogeneous landscapes or complex surfaces, the value of $d\varepsilon$ (Equation 4) may be 2% and $\boldsymbol{F}$ is a shape factor whose mean is 0.55 (Guha et al., 2018; Sobrino et al., 2004)

$$d\varepsilon = (1 - \varepsilon_s)(1 - P_v) F\varepsilon_v \tag{4}$$

The Proportion of vegetation (Pv) is computed from the values of Normalized Difference Vegetation Index (NDVI; Tucker, 1979) according to Carlson and Ripley (1997), Sobrino et al. (2004) and Sobrino et al.(2008) using the following Equation (5)

$$Pv = \left(\frac{NDVI - NDVI_{min}}{NDVI_{max} - NDVI_{min}}\right)2 \tag{5}$$

Where $(NDVI_{min})$ is the minimum NDVI value (0.2) where pixels are considered as bare soil (non-vegetated areas) and $(NDVI_{\max})$ is the maximum NDVI value (0.5) where pixels are considered as dense vegetation. The NDVI (Tucker, 1979) which denotes the presence of living green vegetation was calculated from the Landsat image of each acquired satellite data, using the Near-Infrared (NIR) and Red (R) wavelengths (Equation 6)

$$NDVI = \frac{NIR - RED}{NIR + RED} \tag{6}$$

Furthermore, the land surface emissivity (**ε**) values range between 0.97 and 0.99 (Sobrino et al., 2004). A constant emissivity value of 0.99 is considered when NDVI >0.5 for fully vegetated pixels in the land surface (PV = 1; Sobrino et al., 2004; Sobrino et al.2008). An emissivity value of 0.986 corresponds to a correction value of the equation that is designated for pixels with a NDVI of ≥0.5. An emissivity value of 0.97 is assumed when NDVI <0.2 for bare soil (Sobrino et al., 2004; Sobrino et al.2008). On the other hand, when NDVI >0.2 to <0.5, it represents a mixture area of both bare soil and vegetation pixels. Consequently, the land surface emissivity was determined using the following Equation (7);

$$\varepsilon = 0.004^{*}\mathrm{P_v}{+}0.986 \tag{7}$$

After deriving the emissivity values, the emissivity-corrected LST (°C) values were extracted based on Equation (8).

$$\mathrm{LST} = \left[\frac{T_B}{1 + (\lambda\sigma T_B/(hc))\ln\varepsilon}\right] - 273.15 \tag{8}$$

where LST = land surface temperature, T_B = at-satellite brightness temperature, λ = wavelength of emitted radiance (λ = 10.8 μm for Landsat TIRS Band 10), σ is Boltzmann constant (1.38×10^{-23}J/K), h = Planck's constant (6.626×10^{-34}Js), c = velocity of light (2.998×10^{-8}m/s), ε is the land surface emissivity. The retrieved LST (°C) values were then converted from degrees Kelvin to degrees Celsius (°C) by subtracting 273.15 from the calculated pixel values. The above steps were repeated for all the acquired images from May 2018 to November 2018. Further details on the these steps of computing land surface temperature can be found in Chander et al. (2009).

2.4. Land cover classification

The Landsat 8 OLI data acquired between May 2018 and November 2018 were used for land cover classification. Before obtaining the detailed vegetation (green cover) for each relevant season, we classified first each satellite image data into five land cover categories (i.e., vegetation, grassland, built-up, water, and bareland) based on the supervised image classification approach using the

Support Vector Machine (SVM) classifier algorithm in the Environment for Visualizing Images (ENVI) 5.3 image processing software.

However, only vegetation (green cover) for each acquired data was retained for further analysis. To derive the discrete information of only vegetation (green cover), the classified land cover map was later reclassified into a binary vegetation and non-vegetation. In this case, a value of one and zero was assigned to vegetation and non-vegetation pixels, respectively. Urban green spaces or vegetation in this study consisted of forests, woodlands, shrubland, cropland, park and green land, and street trees. The non-vegetation areas consisted of impervious surfaces and artificial structures that include pavements and built-up areas, transportation, industrial, commercial and residential space, and water and bareland. Furthermore, the accuracy assessment of vegetation classification was conducted using 90 random points within the vegetation class and validated with Google Earth imagery of 2018. The Kappa coefficient was above 0.8 for each acquired date of vegetation classification.

2.5 The landscape connectivity pattern of vegetation

In this study, the Patch Cohesion Index (PCI) (Schumaker, l996) was used to measure the vegetation connectivity (i.e., its connectivity to other urban green spaces) using binary vegetation and non-vegetation maps as input data. Patch Cohesion Index was selected over other distance-based proximity and connectivity indices like Mean Euclidean Nearest Neighbor Distance (ENN_MN) and Proximity Index (PROX), because it is a relatively simple, robust, and parsimonious metric. It is calculated as a range from 0 to 100 and excludes any internal background that may be present in the landscape (McGarigal et al, 2002). The Patch Cohesion Index is computed using the following Equation (9).

$$\text{Patch Cohesion Index} = \left(1\frac{\sum^{p}}{\sum^{(p\sqrt{a})}}\right)\left(1-\frac{1}{\sqrt{N}}\right)^{-1}(100) \tag{9}$$

In equation 9, p is patch perimeter, a is patch area, and N is the number of pixels in the map. The higher the patch cohesion index, the more physically connected, clumped, and aggregated the patch type in its distribution in a landscape and vice versa (McGarigal et al, 2002). The PCI was calculated using the Fragstats 4.2 software.

The PCI of vegetation was further divided into ranges of 10%–30% (less connected vegetation), 30%–50%, 50%–70%, and 70%–100% (more connected vegetation). Less connected vegetation (<0%–30%) is usually associated with highly fragmented nature of vegetation patches that are smaller, isolated, and scattered across the landscape. On the contrary, higher vegetation connectivity (i.e., less isolation of vegetation patches) is associated with a greater proportion of high, contiguous vegetation patches, reflecting shorter distances between the vegetation patches.

2.6 Spatial configuration (dispersed and clustered) patterns of vegetation

The local Moran's I (Anselin, 1995) was used to characterize the spatial configuration patterns of vegetation based on the calculated NDVI of each month and season as input data. As one of the Local Indicators of Spatial Association (LISA), the local Moran's I is effective in characterizing the spatial arrangement or spatial configuration patterns (clustered to dispersed) of land cover at a local scale (Fan & Myint, 2014). The standard formula for local Moran's I is expressed using the following Equation (10).

$$1_i(d) = \frac{x_i - \bar{X}}{\sum_i (x_i - \bar{X})^2}\sum_{\mathrm{j}} w_{ij}(d)(x_j - \bar{X}) \tag{10}$$

Table 2. The threshold of ecological evaluation index using UTFVI.

Urban thermal field variance index	Urban heat island Phenomenon	Ecological evaluation Index
Less than 0	None	Excellent
From 0.000 to 0.005	Weak	Good
From 0.005 to 0.01	Moderate	Normal
From 0.01 to 0.015	Strong	Bad
From 0.015 to 0.02	Stronger	Worse
More than 0.02	Strongest	Worst

where x_i and x_j represent the attribute values at locations i and j, respectively. $\bar{x}$ denotes the average attribute values of all the pixels in the study region. $\{w_{ij}(d)\}$ is a spatial weight matrix where the diagonal elements are all zero, and the off-diagonal elements are either one or zero, depending on whether the corresponding pixels are neighbors. Basically, wij is calculated on the basis of the conceptualized spatial relationship and in reference to d, the distance that defines the neighbors. Therefore, it is often written as wij (d). Therefore, pixels that were located within a distance of d were considered adjacent. The values of local Moran's I index were standardized and normalized to the range of −1 to 1. In this regard, the positive values of Local Moran's I represent highly clustered patterns, while the negative values of the Local Moran's I represent highly dispersed patterns and the values of zero indicate random spatial configuration patterns.

2.7. Computation of the urban thermal field variance index (UTFVI)

In this study, UTFVI was used to compute the ecological evaluation of UHI impacts on the quality of urban life for the city in all seasons. UTFVI was estimated and expressed based on Liu and Zhang (2011) and J. Zhang et al. (2006) using Equation (11).

$$\mathrm{UTFVI} = \frac{T_s - T_{mean}}{T_{mean}} \tag{11}$$

where UTFVI = Urban Thermal Field Variance Index, T_s = LST (°C), represents the surface temperature of a certain point, and T_{mean} = Mean LST (°C), the mean value of the surface temperature of the study area. UTFVI is a relative variable based on the surface temperature, and the higher the value, the stronger the effects of urban heat. The UTFVI was further divided into six different categorical ecological evaluations of UHI levels (Liu & Zhang, 2011; J. Zhang et al., 2006). The thresholds in the six UTFVI levels are shown in Table 2.

2.8. Correlation analysis

The Pearson's product-moment correlation coefficient *(r)*, a parametric statistical method, was applied to quantity the bivariate correlation between LST as the dependent variable and the Patch Cohesion Index (%) and local Moran's I of urban vegetation as the independent variables in each season because our data exhibited a normal Gaussian-distribution. A higher absolute value of Pearson correlation coefficient indicates a stronger correlation. The detailed research methodology used in this study is illustrated in Figure 2.

3. Results

3.1 Seasonal variations of LST

Table 3 shows the descriptive statistics (minimum, maximum, mean and standard deviation) of LST from May to November 2018 in Harare metropolitan city. The spring season (May) had the lowest LST values for all the descriptive statistics. During the spring season (19 May 2018), LST ranged

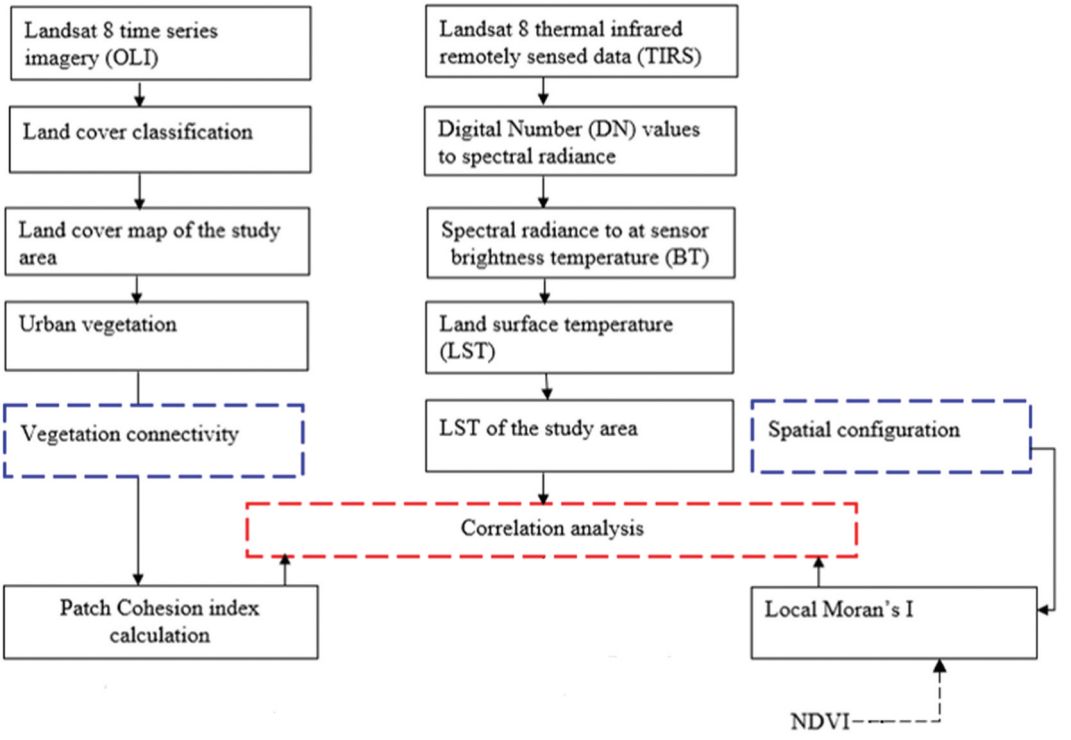

Figure 2. Flowchart of the methodology and the processing steps presented in this study.

from a minimum of 10.79°C to a maximum of 33.61°C. The maximum LST (°C) values of 54°C and 56°C were observed in summer (26 October 2018 and 11 November 2018). The LST in autumn season (August and September) was lower compared to the LST in hot and wet summer seasons (October and November). Generally, LST gradually increased in intensity and spatial extent with change of season from spring, winter, autumn to summer (Table 3 and Figure 3).

The largest ranges of LST were found in the summer (26 October 2018 and 11 November 2018), representing the largest surface temperature contrast of all seasons. It was 30.89°C on 26 October 2018 and 31.86°C on 11 November 2018. The lowest range of 18.3°C LST was observed in the winter (20 June 2018). The spring season (May) and winter month (June) were characterized by low standard deviation of LST (Table 3). On the other hand, the hot (October) and wet (November) summer months were characterized by high standard deviations (Table 3). Visually, the highly vegetated northern part of the city had relatively lower surface temperatures than the densely urbanized and highly built-up areas in the western, eastern, and southern parts of the city (Figure 3).

Table 3. Descriptive statistics of LST (°C) between 19 May 2018 and 11 November 2018.

Acquisition date	Season	Minimum	Maximum	Range	Mean	Std Dev*
19 May 2018	Spring	10.79	33.61	22.82	22.04	1.75
20 June 2018	Winter	17.38	35.68	18.3	24.73	2.22
23 August 2018	Autumn	20.18	45.60	25.42	31.10	2.65
24 September 2018	Autumn	22.16	46.13	23.97	34.63	2.99
26 October 2018	Summer	23.32	54.21	30.89	41.22	4.08
11 November 2018	Summer	25.00	56.86	31.86	43.03	4.42

Std Dev* – Standard Deviation

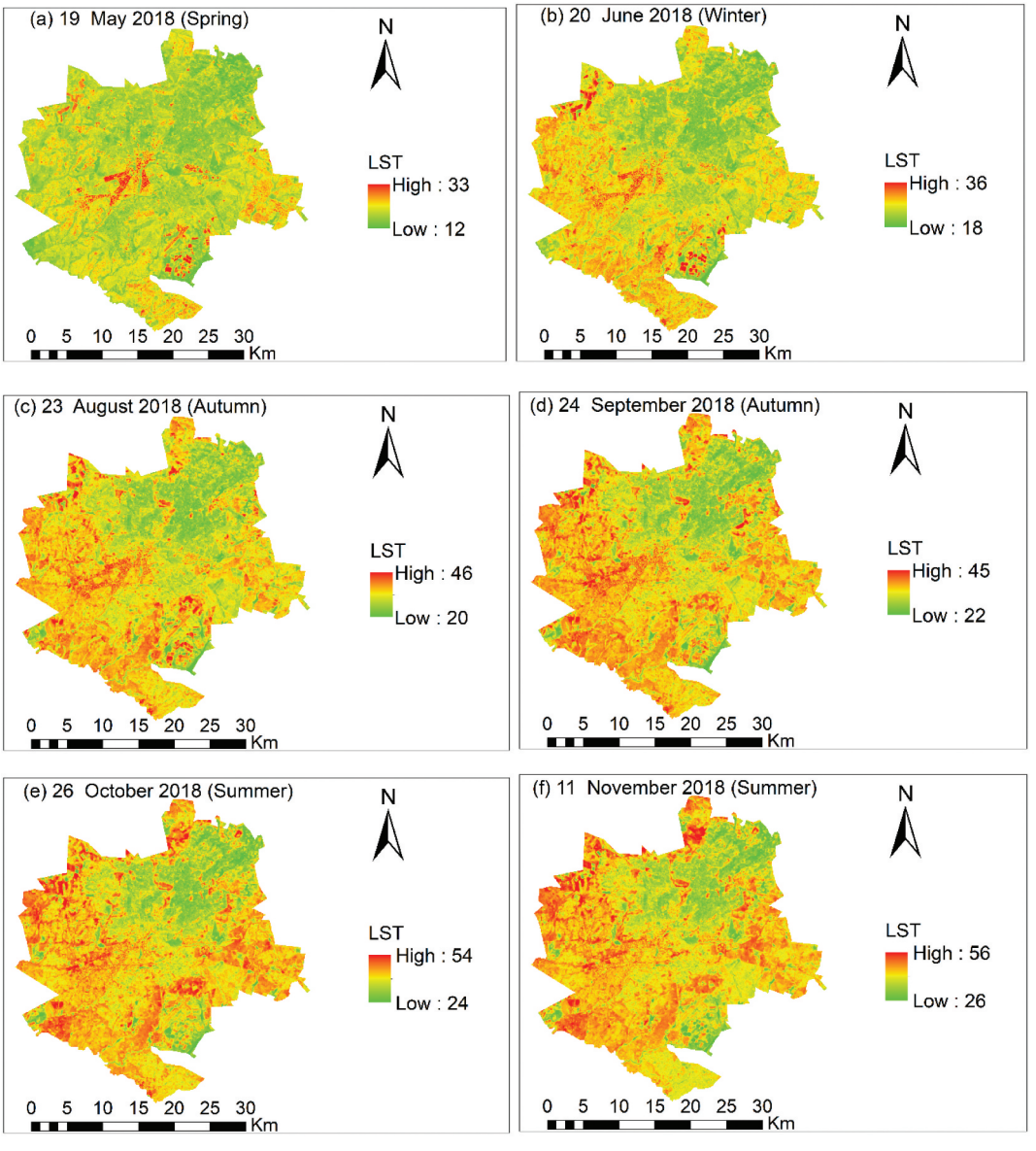

Figure 3. The seasonal variability patterns of LST (°C) in Harare metropolitan city between 19 May 2018 and 11 November 2018. The highly vegetated northern part of the city has relatively low surface temperature than the highly built-up areas in the western, southern and eastern parts of the city.

3.2. Ecological assessment of the city using UTFVI

An ecological assessment of Harare metropolitan city based on UTFVI between 19 May 2018 and 11 November 2018 is shown in Figure 4 and Table 4. Table 4 shows that in all seasons, the city had a moderate percentage of spatial coverage for the excellent category and the worst category of ecological and thermal conditions. The largest portion (52.8%) of Harare metropolitan city experienced optimal thermal conditions (i.e., UTFVI < 0) for living in the spring season (19 May 2018; Table 4), indicating weak urban heat island effects. Generally, the northern part of Harare metropolitan city experienced favorable thermal conditions due to the presence and abundance of vegetation.

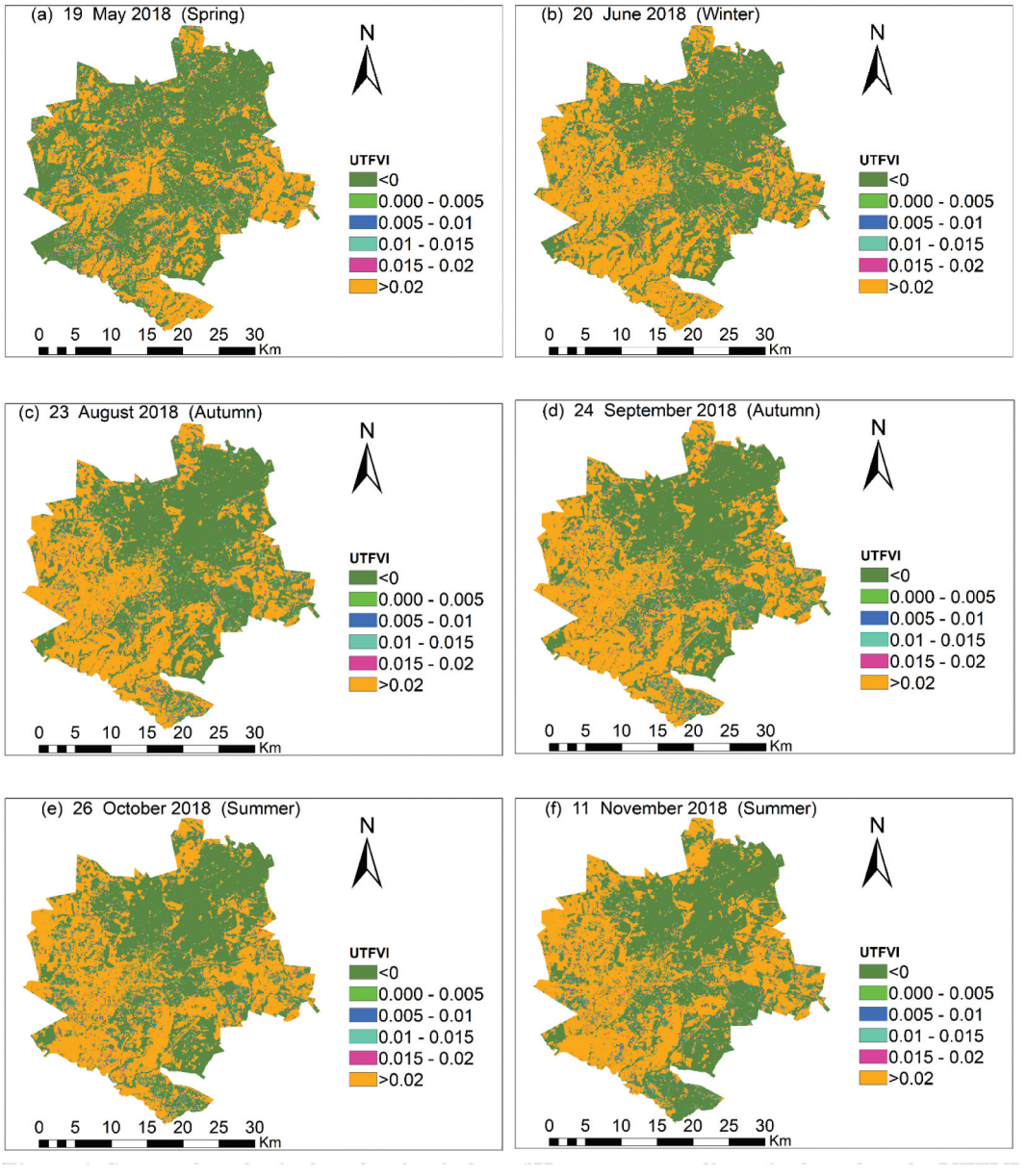

Figure 4. Seasonal ecological evaluation index of Harare metropolitan city based on the UTFVI ranging from the excellent category (UTFVI < 0) and the worst category (UTFVI > 0.020) representing the intensity of UHIs from weak to extremely strong heat islands.

However, the worst category (i.e., UTFVI > 0.020) of the ecological evaluation index, which represents the extremely strong heat islands, was experienced in less than 50% (37%–47%) of the city in all the seasons (Figure 4 and Table 4). This portion extends from the western, eastern, and southern parts of the city. In these areas, most of the land is highly urbanized, with huge concentration of built-up areas intermixed with either bareland or vacant land located in the residential and industrial areas of the city. Comparatively, areas that were characterized by strong UHI effects (i.e., UTFVI > 0.01) were located around built-up areas covering a relatively small portion (2.0%–2.5%) of the city in all seasons. Areas that experienced bad thermal comfort

Table 4. The threshold of ecological evaluation index of Harare metropolitan city between 19 May 2018 and 11 November 2018.

		Percentage of area (%)					
Acquisition date	Season	Excellent	Good	Normal	Bad	Worse	Worst
19 May 2018	Spring	52.80	2.60	2.52	2.45	2.40	37.24
20 June 2018	Winter	47.06	1.91	1.93	2.00	2.04	45.05
23 August 2018	Autumn	45.83	2.23	2.30	2.33	2.39	44.92
24 September 2018	Autumn	43.68	2.23	2.33	2.40	2.46	46.90
26 October 2018	Summer	43.61	2.15	2.24	2.32	2.36	47.32
11 November 2018	Summer	45.46	2.04	2.07	2.11	2.17	46.15

Table 5. Pearson's correlation between LST (°C) and local Moran's I and PCI (COHESION).

Acquisition date	Season	local Moran's I	PCI
19 May 2018	Spring	−0.69	−0.54
20 June 2018	Winter	−0.74	−0.54
23 August 2018	Autumn	−0.74	−0.47
24 September 2018	Autumn	−0.74	−0.57
26 October 2018	Summer	−0.71	−0.59
11 November 2018	Summer	−0.70	−0.58

conditions also ranged between (2.0%–2.5%) of the study area in all seasons. Furthermore, areas that experienced good and normal thermal conditions only covered a small portion (1.9%–2.6%) of the study area in all seasons.

3.3. The effect of spatial configuration of urban vegetation on seasonal LST based on local Moran's I

The Pearson correlation coefficients (r) indicated a moderate to relatively strong and negative relationship between LST and local Moran's I (Table 5). In particular, the correlation coefficients ranged from $r = -0.69$, $p < 0.05$ in spring (19 May 2018) to $r = -0.74$, $p < 0.05$ in both winter (20 June 2018) and autumn seasons (23 August 2018 and 24 September 2018). The results suggest that as local Moran's I for vegetation patterns gets higher (i.e., vegetation patches become more clustered), LST decreases. Therefore, positive and higher spatial clustering of vegetation correlates strongly with lower LST. Conversely, low and negative local Moran's I were associated with dispersed vegetation patches, which tend to increase LST and correlate strongly with higher LST.

3.4 The relationship between vegetation connectivity and seasonal LST

Table 5 indicates a moderate and negative correlation between LST and PCI (%) of vegetation in all four seasons. The Pearson product–moment correlation coefficient (r) between PCI and LST ranged from ($r = -0.47$, $p < 0.05$) in autumn (23 August 2018) to ($r = -0.59$, $p < 0.05$) in hot, dry summer (26 October 2018). This indicates that highly and physically connected vegetation patterns have a strong cooling effect, hence more beneficial in decreasing high LST. As illustrated in Figure 5, in all seasons, the low LST were mainly concentrated in the northern parts of the city, corresponding to the higher vegetation connectivity range (<50%–100%). On the other hand, lower vegetation connectivity (<0%–30%) may contribute to high LST values (Figure 5). Areas with less connected vegetation were found in the western, southern, and eastern side of the city.

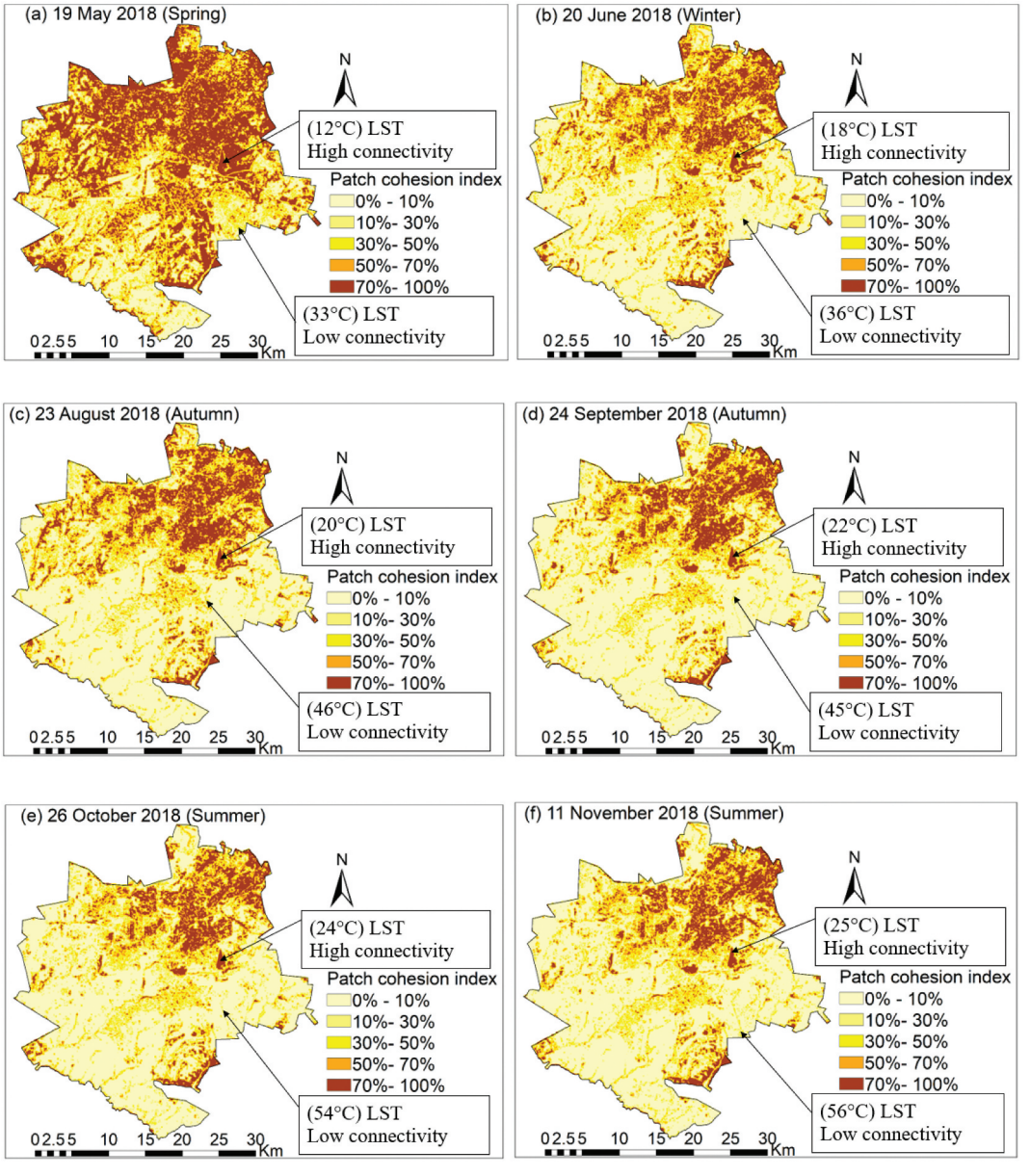

Figure 5. Patch Cohesion Index of vegetation between May 2018 and November 2018 in Harare metropolitan city indicating that higher vegetation connectivity (<50%–100%) are associated with low LST. Less connected vegetation (<0%–30%) are associated with high LST.

4. Discussion

4.1. Spatial variability and seasonal UHI patterns

Our results concur with previous findings including a study by Mushore et al. (2017) that the southern, eastern, and western parts of Harare metropolitan city experience high LST in all seasons, hence stronger UHI. This is because the southern, eastern, and western parts of the city are more densely urbanized than the northern parts. Densely urbanized and built-up areas are associated with higher solar energy absorption (lower albedo) and thermal conductivity and larger heat capacity, leading to higher surface heat storage during the day and hotter summer months

(Memon et al., 2009; S. Peng et al., 2011; Zhou et al., 2011). In Beijing, for instance, higher UHI values have been reported in summer than in other seasons (J.K. Wang et al., 2007; Yang et al., 2010). The low LST experienced in northern part of the city may be due to cooling effects associated with the evapotranspiration and shading provided by of the proportion of urban vegetation (Guha and Govil 2021a).

4.2 Ecological evaluation of the city

The ecological evaluation of Harare metropolitan city indicated that the northern part of Harare metropolitan city experienced favorable thermal conditions (i.e., UTFVI < 0) in all seasons than the heat-stressed western, eastern, and southern parts of the city. Guha et al. (2018) found almost equal proportion of excellent and worst ecological conditions in two cities, Florence and Naples, in Italy. The UHI zones (urban areas) were under severe heat stress when compared to non-UHI areas (vegetation coverage and water bodies) that had excellent thermal conditions. In another study, Dos Santos et al. (2017) examined the thermal ecological conditions of municipality of Vila Velha, in Brazil during 2008–2011, revealing worst ecological conditions in the urbanized areas of the city.

Furthermore, the spatial variability patterns of the eco-environmental conditions of two Asian cities, Beijing of China and Islamabad of Pakistan were compared (Naeem et al., 2018). In both cities, the worst eco-environmental conditions were mainly found in built-areas where the proportion of vegetation cover was very low (Naeem et al., 2018). Overall, all these studies show that in densely built-up areas with less vegetation, the eco-environmental conditions are worse because of stronger urban heat island effects (Dos Santos et al., 2017; Guha et al., 2018; Liu & Zhang, 2011; Naeem et al., 2018). With rapid urban development, the heavily built-up area may worsen the eco-environmental quality conditions of urban areas.

4.3 The effects of spatial configuration of urban green spaces on seasonal LST based on Local Moran's I

Based on a local Moran's I, our findings are consistent with previous studies that indicate that dense and less fragmented patterns of urban vegetation patches are more effective in lowering LST than more fragmented (dispersed) urban vegetation patterns (Fan et al., 2015; Li et al., 2012; J. Peng et al., 2016; Zhang, Zhong, Feng et al., 2009). Clustered green spaces were significant in reducing both daytime and nighttime surface temperatures in geographical regions with dry and warm summers in Phoenix and Portland in the United States of America (C. Wang et al., 2019). Small, isolated green spaces are associated with high thermal load and are unlikely to produce significant cooling effects (Bao et al., 2016). Furthermore, such areas maintain lower rates of evapotranspiration, subsequently increasing summer daytime LST and UHI effects.

In our study, visual inspection of the maps showed that low LST were recorded in the northern parts of Harare. This was due to the existence of contiguous vegetation patches. Contiguous vegetation patches significantly reduce LST through evapotranspiration and shading of the surface, thereby reducing the sensible heat emitted from the surface and efficiently mitigating the UHI effects (Myint et al., 2013; S. Peng et al., 2011; Zhou et al., 2014). Such cooler conditions may be of particular importance to the elderly who are sensitive to stressful urban thermal environments. The spatial patterns of grasses and trees based on local Moran's I were reported to have significantly stronger negative correlation in summer than in winter seasons, suggesting that the rational design of urban vegetation patterns can induce significant cooling effects in summer season (Fan et al., 2015).

Although a positive relationship between clustered urban vegetation and LST was not established and reported in this study, the actual impact of the spatial clustering of urban green spaces on LST may actually be influenced by other factors including the background climate (cloud cover,humidity and precipitation levels, velocity and wind patterns). For instance, during the hot and dry summer season, in tropical African cities such as Harare metropolitan city, the absence of strong

winds and pressure and low annual rainfall could lower the overall evapotranspiration rate and offset the cooling benefits associated with urban vegetation. Such research findings have been reported for drier climates such as Los Angeles or Phoenix in Uinted Statems of America (C. Wang et al., 2019) and Asian cities such as Hong Kong (Tan et al., 2016) and Singapore (Hwang et al., 2015). This, therefore, may indicate that other factors like urban form (compact versus dispersed) and background climate should be considered to better understand the impact of spatial configuration of urban vegetation on LST.

4.4 The relationship between vegetation connectivity and seasonal LST

Our results showed a negative relationship between PCI and LST in all seasons, implying that well-connected urban vegetation patches are more beneficial in decreasing LST in all seasons. Similar to our findings, Kim et al. (2016) measured the spatial configurations and landscape structures of neighborhood trees and forests in single-family residential areas in Austin, Texas, and showed that the PCI had a negative relationship with LST. However, contradictory results have been reported in Zhou et al. (2011) where the impact of clustered patterns of woody vegetation LST using the Mean Nearest Neighbor Distance (MNND) was found to elevate LST. The reported results could have been due to the confounding effects of the high correlation between MNND and the vegetation fraction (Fan et al., 2015).

The PCI typically has a direct relationship with the ecological flows of the landscape (McGarigal, 2002), with a higher value representing a more physically connected spatial patterns of urban vegetation patches. Zhang, Zhong, Feng et al. (2009) noted that the physical connectivity of urban vegetation may be responsible for facilitating the energy flows and exchange in a landscape associated with land surface characteristics, i.e., albedo and evapotranspiration among land cover features like vegetation, which can lead to a lower mean LST. Higher connected vegetation patches lower LST and act as heat sinks, which exert cooling effects on the surrounding environment (Chen et al., 2016; W. F. Li et al., 2017). However, urban vegetation is fragmented by human infrastructures, such as settlements, transport networks, and commercial buildings, leading to low vegetation connectivity and high vegetation fragmentation. Lower vegetation connectivity promotes warmer and higher surface temperatures and acts as heat sources.

4.5 Theoretical and practical implications for urban planning and management

The study showed that PCI of vegetation had a moderate negative relationship (r= −0.47 to r= −0.59), while local Moran's I of vegetation had relatively strong negative correlations (r = −0.69 to r = −0.74) with LST. The difference between the two indices (local Moran's I and PCI) on their impact on LST has partly to do with the way they were derived and computed from satellite data. In this study, the Local Moran's I index was computed on continuous vegetation data, NDVI, while PCI was derived from discrete or classified vegetation data. Fan and Myint (2014) showed that the continuous indices like Local Moran's I index show great potential in effectively characterizing the spatial patterns (landscape composition and abundance of dominant patches) of any land cover type or a combination of different land cover types without the need of classifying high-resolution satellite data. Unlike other discrete methods, Local Indicators of Spatial Association (LISA) indices like local Moran's I derived from satellite image data permit also the accurate extraction of feature abundance and spatial configuration of urban vegetation at a local scale while preserving as many fine spatial details (Fan & Myint, 2014).

The results of this study can provide important insights into landscape design, urban planning and management particularly in cities experiencing rapid urbanization on how to arrange and optimize urban vegetation (lawns, grass, and trees) in order to maximize the cooling benefits. LST can be significantly increased or decreased by different spatial arrangements or configuration and landscape connectivity of vegetation cover whether they are physically isolated, connected, or

clustered. For instance, reducing vegetation fragmentation by creating well-connected green space networks and maintaining large patch sizes instead of small, isolated vegetation patches reduces LST.

4.6 Limitations of the study

In this study, we have developed a useful framework for examining the eco-environmental quality or thermal well-being and the impact of the spatial configuration and landscape connectivity patterns of urban vegetation based on seasonal LST for Harare metropolitan city. However, this research has some limitations. Firstly, the present study examined the seasonal variations of landscape pattern of urban vegetation on LST only in 1 year which is rather limited considering the annual variations. Further research should examine the impact of landscape patterns of urban vegetation on the seasonal LST in different years. Furthermore, this study did not differentiate the materials that comprise vegetation (e.g., street trees, grass/lawn). The impacts of the three-dimensional structure of urban vegetations such as tree height and canopy at the fine-scale should also be included to better understand their impact on spatial configuration on seasonal LST. Future research should focus more on examining the relationships between seasonal LST by differentiating the materials that comprise vegetation including tree height.

Due to the small patch size and highly heterogeneous nature of urban vegetation features such as alleys, lawns, parks, private gardens and single trees, remotely sensed data with medium and coarse resolution may fail to depict the fine-scale complexity and detailed examination of spatial configurations and landscape connectivity of green spaces on the urban surface temperature. Hence, further studies need to be conducted by considering the urban land cover data and information acquired from high resolution remote sensing images. Lastly, we used remotely sensed daytime LST data to represent the urban thermal environment in this study. However, in a city, the relationship between LST and air temperature may vary during daytime and nighttime. In situ observations from ground-based weather stations and sensors should be made to quantify the relationship between LST and air temperature at different times.

5. Conclusion

The results of the study showed that approximately more 50% of Harare metropolitan city experiences optimal thermal condition (i.e., UTFVI < 0) for living in the spring season when compared to around 40% of the study area that experiences optimal thermal condition during the hot and dry season (October). The study further showed that the worse eco-environmental conditions (i.e., UTFVI > 0.020) were mainly experienced in approximately 37%–47% of the city especially in the densely built-up areas with less vegetation in the southern, eastern, and western parts of the city. The moderate (r= −0.47 to r= −0.59) and relatively strong negative correlations (r = −0.69 to r = −0.74) of PCI and Local Moran's I index with LST, respectively, imply that clustered and highly connected rather than isolated or fragmented urban green spaces are more beneficial in decreasing LST in all seasons. Our results have important theoretical, scientific, and policy implications for landscape and urban planning, particularly in rapidly urbanizing tropical African cities, where available land area for increased urban expansion and greenery space is limited and shrinking. Optimizing the spatial configuration and landscape connectivity patterns of urban vegetation should be encouraged in order to maintain a rational balance between the sustainability of cities to improve urban thermal comfort, maintain livability, habitability, and healthier favorable eco-environmental quality conditions.

Disclosure statement

No potential conflict of interest was reported by the author(s).

Funding

This research work was supported and funded by the Department of Science and Technology (DST) and National Research Foundation (NRF) of South Africa Chair in Land Use Planning and Management [84157].

Notes on contributors

Pedzisai Kowe is an urban climate and landscape ecology researcher and lecturer at Midlands State University, Gweru, Zimbabwe. Dr. Pedzisai Kowe got his Doctor of Philosophy (PhD) in Environmental Science (Remote Sensing) from the College of Agriculture, Engineering and Science at University of KwaZulu Natal, South Africa. He holds a MSc in Geoinformation Science and Earth Observation (University of Twente, Enschede, The Netherlands). Before joining the Midlands State University, he was a Research Scientist (Remote Sensing and GIS specialist) at the Geoinformation Science and Remote Sensing Institute of the Scientific and Industrial Research and Development Centre (SIRDC), Harare, Zimbabwe's premier technology centre. Dr. Pedzisai Kowe integrates field observations, geospatial technologies, remote sensing and ecological modelling to understand the structure of urban socio-ecological systems, and its link to urban growth, urban transport systems land surface temperature and urban climate.

Onisimo Mutanga is a full Professor and SARChI Chair on Land use Planning at the University of KwaZulu Natal (Pietermaritzburg Campus), South Africa. He is an NRF B – rated Scientist with more than 350 scientific publications, 13000 citations and an H index of 53. His expertise lies in understanding the current state of vegetation (including agricultural crops) in the face of global change by using earth observation data and methods. He integrates landscape ecology techniques, biodiversity conservation and remote sensing data to quantify and understand the impact of forest fragmentation, pests and diseases and invasive species on agricultural and natural ecosystems.

John Odindi is a Professor in the School of Agriculture, Earth and Environmental Studies at University of KwaZulu Natal (Pietermaritzburg Campus) His expertise lies in understanding the impact of land cover/land use, urban growth on urban heat island in African cities and maping alien and indigenous vegetation using remotely sensed data. Has published more than with more than 120 scientific publications.

Timothy Dube is a full Professor at the Department of Earth Sciences, University of Western Cape, South Africa and a National Research Foundation of South Africa (NRF) rated researcher with interest in GIScience and Earth Observation (EO) applications in environmental and water resources management. Has published more than 200 scientific publications. His research is inclined towards the use of cutting-edge satellite and in-situ earth observation technologies in tracking the impacts of climate change and in monitoring water resources and the environment. Together, with various experts drawn from European institutions, Professor Timothy Dube has been involved in intensive earth observation technologies training and capacity building across different institutions of higher learning and research in Southern Africa.

References

Akbari, H., Pomerantz, M., & Taha, H. (2001). Cool surfaces and shade trees to reduce energy use and improve air quality in urban areas. *Solar Energy*, *70*(3), 295–310. https://doi.org/10.1016/S0038-092X(00)00089-X

Anderson, G. B., & Bell, M. L. (2010). Heat waves in the United States: Mortality risk during heat waves and effect modification by heat wave characteristics in 43 US communities. *Environmental Health Perspectives*, *119*(2), 210–218. https://doi.org/10.1289/ehp.1002313

Anselin, L. (1995). Local indicators of spatial association—LISA. *Geographical Analysis*, *27*(2), 93–115. https://doi.org/10.1111/j.1538-4632.1995.tb00338.x

Bao, T., Li, X., Zhang, J., Zhang, Y., & Tian, S. (2016). Assessing the distribution of urban green spaces and its anisotropic cooling distance on urban heat island pattern in Baotou, China. *ISPRS International Journal of Geo-Information*, *5*(2), 12. https://doi.org/10.3390/ijgi5020012

Cao, X., Onishi, A., Chen, J., & Imura, H. (2010). Quantifying the cool island intensity of urban parks using ASTER and IKONOS data. *Landscape and Urban Panning*, *96*(4), 224–231. https://doi.org/10.1016/j.landurbplan.2010.03.008

Carlson, T. N., Gillies, R. R., & Perry, E. M. (1994). A method to make use of thermal infrared temperature and NDVI measurements to infer surface soil water content and fractional vegetation cover. *Remote Sensing Reviews*, *9*(1–2), 161–173. https://doi.org/10.1080/02757259409532220

Carlson, T. N., & Ripley, D. A. (1997). On the relation between NDVI, fractional vegetation cover, and leaf area index. *Remote Sensing of Environment*, *62*(3), 241–252. https://doi.org/10.1016/S0034-4257(97)00104-1

Chander, G., & Markham, B. (2003). Revised Landsat-5 TM radiometric calibration procedures and post calibration dynamic ranges. *IEEE Transactions on Geoscience and Remote Sensing*, *41*(11), 2674–2677. https://doi.org/10.1109/TGRS.2003.818464

Chander, G., Markham, B. L., & Helder, D. L. (2009). Summary of current radiometric calibration coefficients for Landsat MSS, TM, ETM+, and EO-1 ALI sensors. *Remote Sensing of Environment*, *113*(5), 893–903. https://doi.org/10.1016/j.rse.2009.01.007

Chen, A., Sun, R., & Chen, L. (2012). Studies on urban heat island from a landscape pattern view: A review. *Shengtai Xuebao/Acta Ecologica Sinica*, *32*(14), 4553–4565. https://doi.org/10.5846/stxb201106280965

Chen, A., Zhao, X., Yao, L., & Chen, L. (2016). Application of a new integrated landscape index to predict potential urban heat islands. *Ecological Indicators*, *69*, 828–835. https://doi.org/10.1016/j.ecolind.2016.05.045

Connors, J. P., Galletti, C. S., & Chow, W. T. (2013). Landscape configuration and urban heat island effects: Assessing the relationship between landscape characteristics and land surface temperature in Phoenix, Arizona. *Landscape Ecology*, *28*(2), 271–283. https://doi.org/10.1007/s10980-012-9833-1

Dos Santos, A. R., de Oliveira, F. S., da Silva, A. G., Gleriani, J. M., Gonçalves, W., Moreira, G. L., Silva, F. G., Branco, E. R. F., Moura, M. M., da Silva, R. G., Juvanhol, R. S., de Souza, K. B., Ribeiro, C. A. A. S., de Queiroz, V. T., Costa, A. V., Lorenzon, A. S., Domingues, G. F., Marcatti, G. E., de Castro, N. L. M., … Mota, P. H. S. (2017). Spatial and temporal distribution of urban heat islands. *Science of the Total Environment*, *605*, 946–956. https://doi.org/10.1016/j.scitotenv.2017.05.275

Fan, C., & Myint, S. (2014). A comparison of spatial autocorrelation indices and landscape metrics in measuring urban landscape fragmentation. *Landscape and Urban Planning*, *121*, 117–128. https://doi.org/10.1016/j.landurbplan.2013.10.002

Fan, C., Myint, S. W., & Zheng, B. (2015). Measuring the spatial arrangement of urban vegetation and its impacts on seasonal surface temperatures. *Progress in Physical Geography*, *39*(2), 199–219. https://doi.org/10.1177/0309133314567583

Fischer, E. M., Seneviratne, S. I., Lüthi, D., & Schär, C. (2007). Contribution of land-atmosphere coupling to recent European summer heat waves. *Geophysical Research Letters*, *34*(6). https://doi.org/10.1029/2006GL029068

Guha, S. (2021). Dynamic seasonal analysis on LST-NDVI relationship and ecological health of Raipur City, India. *Ecosystem Health and Sustainability*, *7*(1), 1927852. https://doi.org/10.1080/20964129.2021.1927852

Guha, S., & Govil, H. (2021a). Annual assessment on the relationship between land surface temperature and six remote sensing indices using Landsat data from 1988 to 2019. *Geocarto International* 37(15), 1–20. doi:10.1080/10106049.2021.1886339.

Guha, S., Govil, H., Dey, A., & Gill, N. (2018). Analytical study of land surface temperature with NDVI and NDBI using Landsat 8 OLI and TIRS data in Florence and Naples city, Italy. *European Journal of Remote Sensing*, *51*(1), 667–678. https://doi.org/10.1080/22797254.2018.1474494

Hwang, Y. H., Lum, Q. J. G., & Chan, Y. K. D. (2015). Micro-scale thermal performance of tropical urban parks in Singapore. *Building and Environment*, *94*, 467–476. https://doi.org/10.1016/j.buildenv.2015.10.003

Jenerette, G. D., Harlan, S. L., Brazel, A., Jones, N., Larsen, L., & Stefanov, W. L. (2007). Regional relationships between surface temperature, vegetation, and human settlement in a rapidly urbanizing ecosystem. *Landscape Ecology*, *22*(3), 353–365. https://doi.org/10.1007/s10980-006-9032-z

Kamusoko, C., Gamba, J., & Murakami, H. (2013). Monitoring urban spatial growth in Harare metropolitan province, Zimbabwe. *Advances in Remote Sensing*, *2*(4), 322–331. https://doi.org/10.4236/ars.2013.24035

Kim, J. H., Gu, D., Sohn, W., Kil, S. H., Kim, H., & Lee, D. K. (2016). Neighborhood landscape spatial patterns and land surface temperature: An empirical study on single-family residential areas in Austin, Texas. *International Journal of Environmental Research and Public Health*, *13*(9), 880. https://doi.org/10.3390/ijerph13090880

Kong, F., Yin, H., James, P., Hutyra, L. R., & He, H. S. (2014). Effects of spatial pattern of greenspace on urban cooling in a large metropolitan area of eastern China. *Landscape and Urban Planning*, *128*, 35–47. https://doi.org/10.1016/j.landurbplan.2014.04.018

Li, W. F., Cao, Q. W., Lang, K., & Wu, J. S. (2017). Linking potential heat source and sink to urban heat island: Heterogeneous effects of landscape pattern on land surface temperature. *Science of the Total Environment*, *586*, 457–465. https://doi.org/10.1016/j.scitotenv.2017.01.191

Li, X., Li, W., Middel, A., Harlan, S. L., Brazel, A. J., & Turner Ii, B. L. (2016). Remote sensing of the surface urban heat island and land architecture in Phoenix, Arizona: Combined effects of land composition and configuration and cadastral–demographic–economic factors. *Remote Sensing of Environment*, *174*, 233–243. https://doi.org/10.1016/j.rse.2015.12.022

Li, J., Song, C., Cao, L., Zhu, F., Meng, X., & Wu, J. (2011). Impacts of landscape structure on surface urban heat islands: A case study of Shanghai, China. *Remote Sensing of Environment*, *115*(12), 3249–3263. https://doi.org/10.1016/j.rse.2011.07.008

Li, H., & Wu, J. (2004). Use and misuse of landscape indices. *Landscape Ecology*, *19*(4), 389–399. https://doi.org/10.1023/B:LAND.0000030441.15628.d6

Li, X., Zhou, W., Ouyang, Z., Xu, W., & Zheng, H. (2012). Spatial pattern of greenspace affects land surface temperature: Evidence from the heavily urbanized Beijing metropolitan area, *China*. *Landscape Ecology*, *27*(6), 887–898. https://doi.org/10.1007/s10980-012-9731-6

Liu, L., & Zhang, Y. (2011). Urban heat island analysis using the Landsat TM data and ASTER data: A case study in Hong Kong. *Remote Sensing*, *3*(7), 1535–1552. https://doi.org/10.3390/rs3071535

Mallick, J., Kant, Y., & Bharath, B. D. (2008). Estimation of land surface temperature over Delhi using Landsat-7 ETM +. *J. Ind. Geophys. Union*, *12*(3), 131–140.

McGarigal, K., Cushman, SA, Neel, MC, Ene, E. 2002. *Fragstats: spatial pattern analysis program for categorical maps*. http://www.umass.edu/landeco/research/fragstats/fragstats.Html

Memon, R. A., Leung, D. Y., & Liu, C. H. (2009). An investigation of urban heat island intensity (UHII) as an indicator of urban heating. *Atmospheric Research*, *94*(3), 491–500. https://doi.org/10.1016/j.atmosres.2009.07.006

Mushore, T. D., Mutanga, O., Odindi, J., & Dube, T. (2017). Linking major shifts in land surface temperatures to long term land use and land cover changes: A case of Harare, Zimbabwe. *Urban Climate*, *20*, 120–134. https://doi.org/10.1016/j.uclim.2017.04.005

Myint, S. W., Wentz, E. A., Brazel, A. J., & Quattrochi, D. A. (2013). The impact of distinct anthropogenic and vegetation features on urban warming. *Landscape Ecology*, *28*(5), 959–978. https://doi.org/10.1007/s10980-013-9868-y

Naeem, S., Cao, C., Waqar, M. M., Wei, C., & Acharya, B. K. (2018). Vegetation role in controlling the ecoenvironmental conditions for sustainable urban environments: A comparison of Beijing and *Islamabad*. *Journal of Applied Remote Sensing*, *12*(1), 016013. https://doi.org/10.1117/1.JRS.12.016013

Nor, A. N. M., Corstanje, R., Harris, J. A., & Brewer, T. (2017). Impact of rapid urban expansion on green space structure. *Ecological Indicators*, *81*, 274–284. https://doi.org/10.1016/j.ecolind.2017.05.031

Oke, T. R. (1982). The energetic basis of the urban heat island. *Quarterly Journal of the Royal Meteorological Society*, *108*(455), 1–24.

Peng, S., Piao, S., Ciais, P., Friedlingstein, P., Ottle, C., Bréon, F. M., Nan, H., Zhou, L., & Myneni, R. B. (2011). Surface urban heat island across 419 global big cities. *Environmental Science and Technology*, *46*(2), 696–703. https://doi.org/10.1021/es2030438

Peng, J., Xie, P., Liu, Y., & Ma, J. (2016). Urban thermal environment dynamics and associated landscape pattern factors: A case study in the Beijing metropolitan region. *Remote Sensing of Environment*, *173*, 145–155. https://doi.org/10.1016/j.rse.2015.11.027

Schumaker, N. H. (1996). Using landscape indices to predict habitat connectivity. *Ecology*, *77*(4), 1210–1225. https://doi.org/10.2307/2265590

Sobrino, J. A., Jimenez-Munoz, J. C., & Paolini, L. (2004). Land surface temperature retrieval from LANDSAT TM 5. *Remote Sensing of Environment*, *90*(4), 434–440. https://doi.org/10.1016/j.rse.2004.02.003

Sobrino, J. A., Jiménez-Muñoz, J. C., Sòria, G., Romaguera, M., Guanter, L., Moreno, J., & Martínez, P. (2008). Land surface emissivity retrieval from different VNIR and TIR sensors. *IEEE Transactions on Geoscience and Remote Sensing*, *46*(2), 316–327. https://doi.org/10.1109/TGRS.2007.904834

Tan, Z., Lau, K. K. L., & Ng, E. (2016). Urban tree design approaches for mitigating daytime urban heat island effects in a high-density urban environment. *Energy and Buildings*, *114*, 265–274. https://doi.org/10.1016/j.enbuild.2015.06.031

Tucker, C. J. (1979). Red and photographic infrared linear combinations for monitoring vegetation. *Remote Sensing of Environment*, *8*(2), 127–150. https://doi.org/10.1016/0034-4257(79)90013-0

Uuemaa, E., Mander, Ü., & Marja, R. (2013). Trends in the use of landscape spatial metrics as landscape indicators: A review. *Ecological Indicators*, *28*, 100–106. https://doi.org/10.1016/j.ecolind.2012.07.018

Voogt, J. A., & Oke, T. R. (2003). Thermal remote sensing of urban climates. *Remote Sensing of Environment*, *86*(3), 370–384. https://doi.org/10.1016/S0034-4257(03)00079-8

Wang, C., Li, Y., Myint, S. W., Zhao, Q., & Wentz, E. A. (2019). Impacts of spatial clustering of urban land cover on land surface temperature across Köppen climate zones in the contiguous United States. *Landscape and Urban Planning*, *192*, 103668. https://doi.org/10.1016/j.landurbplan.2019.103668

Wang, J. K., Wang, K. C., & Wang, P. C. (2007). Urban heat (or cool) island over Beijing from MODIS land surface temperature. *Journal of Remote Sensing-Beijing-*, *11*(3), 330.

Weng, Q., Lu, D., & Schubring, J. (2004). Estimation of land surface temperature–vegetation abundance relationship for urban heat island studies. *Remote Sensing of Environment*, *89*(4), 467–483. https://doi.org/10.1016/j.rse.2003.11.005

Yang, F., Lau, S. S., & Qian, F. (2010). Summertime heat island intensities in three high-rise housing quarters in inner-city Shanghai China: Building layout, density and greenery. *Building and Environment*, *45*(1), 115–134. https://doi.org/10.1016/j.buildenv.2009.05.010

Yao, L., Sun, S., song, C., Li, J., Xu, W., & Xu, Y. (2021). Understanding the spatiotemporal pattern of the urban heat island footprint in the context of urbanization, a case study in Beijing, China. *Applied Geography*, *133*, 102496. https://doi.org/10.1016/j.apgeog.2021.102496

Zhang, Y., Balzter, H., Zou, C., Xu, H., & Tang, F. (2015). Characterizing bi-temporal patterns of land surface temperature using landscape metrics based on sub-pixel classifications from Landsat TM/ETM+. *International Journal of Applied Earth Observation and Geoinformation*, *42*, 87–96. https://doi.org/10.1016/j.jag.2015.06.007

Zhang, X., Friedl, M. A., Schaaf, C. B., Strahler, A. H., Hodges, J. C., Gao, F., Reed, B. C., & Huete, A. (2003). Monitoring vegetation phenology using MODIS. *Remote Sensing of Environment*, *84*(3), 471–475. https://doi.org/10.1016/S0034-4257(02)00135-9

Zhang, Y., Odeh, I. O., & Han, C. (2009). Bi-temporal characterization of land surface temperature in relation to impervious surface area, NDVI and NDBI, using a sub-pixel image analysis. *International Journal of Applied Earth Observation and Geoinformation*, *11*(4), 256–264. https://doi.org/10.1016/j.jag.2009.03.001

Zhang, J., Wang, Y., & Li, Y. (2006). A C++ program for retrieving land surface temperature from the data of Landsat TM/ETM+ band6. *Computers & Geosciences*, *32*(10), 1796–1805. https://doi.org/10.1016/j.cageo.2006.05.001

Zhang, X., Zhong, T., Feng, X., & Wang, K. (2009). Estimation of the relationship between vegetation patches and urban land surface temperature with remote sensing. *International Journal of Remote Sensing*, *30*(8), 2105–2118. https://doi.org/10.1080/01431160802549252

Zheng, B., Myint, S. W., & Fan, C. (2014). Spatial configuration of anthropogenic land cover impacts on urban warming. Landscape and Urban Planning, 130, 104–111. doi: 10.1016/.j.landurbplan.2014.07.001

Zhibin, R., Haifeng, Z., Xingyuan, H., Dan, Z., & Xingyang, Y. (2015). Estimation of the relationship between urban vegetation configuration and land surface temperature with remote sensing. *Journal of the Indian Society of Remote Sensing*, *43*(1), 89–100. https://doi.org/10.1007/s12524-014-0373-9

Zhou, W., Huang, G., & Cadenasso, M. L. (2011). Does spatial configuration matter? Understanding the effects of land cover pattern on land surface temperature in urban landscapes. *Landscape and Urban Planning*, *102*(1), 54–63. https://doi.org/10.1016/j.landurbplan.2011.03.009

Zhou, W., Qian, Y., Li, X., Li, W., & Han, L. (2014). Relationships between land cover and the surface urban heat island: Seasonal variability and effects of spatial and thematic resolution of land cover data on predicting land surface temperatures. *Landscape Ecology*, *29*(1), 153–167. https://doi.org/10.1007/s10980-013-9950-5

Zimstat. (2022). *ZIMBABWE POPULATION CENSUS 2022*, National Report. http://www.zimstat.co.zw/sites/wp-content/uploads/2022/07/Census2022_Preliminary_Report.pdf